Geophysical Research Letters

RESEARCH LETTER
10.1029/2024GL110762

Key Points:

- WRF simulations significantly overestimate snow amount and delay snow phenology on the Tibetan Plateau (TP)
- Snowfall bias is not always transformable into snow amount bias, depending on snow phenology
- Complex relationship between snow amount and surface albedo restricts the transformation of wet to cold bias on the TP

Supporting Information:

Supporting Information may be found in the online version of this article.

Correspondence to:
W. Guo,
guowd@nju.edu.cn

Citation:
Miao, X., Guo, W., Hu, X., Wang, L., Li, Y., & Li, W. (2024). Divergent transformation of wet to cold bias on the Tibetan Plateau in climate models during snow season. *Geophysical Research Letters*, *51*, e2024GL110762. https://doi.org/10.1029/2024GL110762

Received 11 JUN 2024
Accepted 19 AUG 2024

Divergent Transformation of Wet to Cold Bias on the Tibetan Plateau in Climate Models During Snow Season

Xin Miao[1,2], Weidong Guo[1], Xinyun Hu[1], Le Wang[1], Yizhuo Li[1], and Wenkai Li[3]

[1]School of Atmospheric Sciences, Nanjing University, Nanjing, China, [2]Frontiers Science Center for Critical Earth Material Cycling, Nanjing University, Nanjing, China, [3]School of Atmospheric Sciences, Nanjing University of Information Science and Technology, Nanjing, China

Abstract Wet and cold biases on the Tibetan Plateau (TP) commonly exist in global and regional climate simulations. Previous studies have explored the possible causes of wet and cold biases and contributed to reducing these biases. However, the connection between wet and cold biases remains insufficiently addressed. Our research indicates that the TP wet bias converts into positive snow amount bias not continually but efficiently and concentratedly, under the control of snow phenology in different regions. Furthermore, the complex relationship between snow amount, snow coverage and surface albedo restricts the transformation of snow amount to surface albedo bias, and thus to cold bias. Our research highlights the spatio-temporally divergent transformation of wet to cold bias on the TP during snow season, providing a novel perspective to understand the intrinsic connection between wet and cold biases and improve climate simulations on the TP.

Plain Language Summary Due to the harsh environment, observational data are limited on the Tibetan Plateau (TP), so climate model is one of necessary tools for climate researches. However, both global and regional climate models generally overestimate precipitation (wet bias) and underestimate near surface air temperature (cold bias) on the TP. Previous studies have pointed out the possible causes of the wet and cold biases, and partly reduced these biases, leaving the connection between these biases unaddressed. Our study finds that the conversion of wet to cold bias during snow season is divergent in different areas of the TP. Under the control of snow duration in different areas, the wet bias efficiently and concentratedly transforms into larger snow amount. Furthermore, the complex relationship between snow amount, snow coverage and surface albedo restricts the transformation of snow amount to surface albedo bias, and thus to cold bias. We reveal the spatio-temporally divergent transformation of wet to cold bias on the TP during snow season, and these conclusions will contribute to a better improvement of snow and climate modeling on the TP.

1. Introduction

The Tibetan Plateau (TP), the highest plateau on Earth and often referred to as the "Third Pole", exerts significant influence on the weather and climate of surrounding and downstream areas through its mechanical and thermal effects (Duan & Wu, 2005; Hu et al., 2016; Wan et al., 2017; Wang et al., 2014; Wu et al., 2007; Wu & Zhang, 1998; Yeh, 1950). Due to the harsh environment, in situ observations are insufficient to meet the need of climate researches on the TP, making satellite data and climate models necessary tools.

However, the "cold bias" (negative surface air temperature bias) and "wet bias" (positive precipitation bias) on the TP commonly exist in global and regional climate simulations (Cui et al., 2021; Gao et al., 2015; Meng et al., 2018; Su et al., 2013; Yu et al., 2015; Zhu & Yang, 2020). Previous studies have suggested that the wet bias may result from factors such as coarse spatial resolution, cumulus schemes, and complex topography on the TP (Duan et al., 2013; Gao et al., 2018; Gu et al., 2022; Kukulies et al., 2021; Li et al., 2020; Yang et al., 2018; Zhou et al., 2019, 2021), while the cold bias could be attributed to precipitation ice radiative effects and elevation bias (Lee et al., 2019; Salunke et al., 2019; Yue et al., 2021). Moreover, seasonal snow covers the majority of TP during cold seasons, greatly affecting the water cycle and surface energy budget. Therefore, biases in snow simulation highly likely contributes to the cold bias on the TP during snow season (Chen et al., 2017; Lalande et al., 2021; Miao et al., 2022; Usha et al., 2020).

Previous researches have attributed and partially corrected the wet and cold biases, yet the connection between them remains inadequately addressed. During snow season, the overestimated snowfall (wet bias) leads to excessive snow cover (Gao et al., 2020; Miao et al., 2024; Orsolini et al., 2019), potentially inducing a cold bias by influencing surface albedo. However, it remains unclear whether this bias transformation is efficient and continuous. We aim to investigate the role of snow cover in the connection between the wet and cold biases in TP climate simulations.

In this study, we analyze the annual cycle of snow cover changes on the TP using satellite observations, and evaluate the WRF model's capacity to simulate the TP snow phenology. We further investigate the relationship between simulations biases in snowfall and surface snow amount on the TP. Finally, we explore the divergent transformation of wet bias to cold bias in different regions of the TP during snow season.

2. Data and Methods

2.1. Data and Model

In this study, we use three snow data sets to characterize snow and validate simulations on the TP, including a 500 m daily cloudless snow cover fraction (SCF) data set (Tang et al., 2013), a 0.05° daily snow depth (SD) data set (Yan et al., 2021) and a 0.01° daily snow water equivalent data set (Yan & Zhang, 2022). We employ the 8-day surface albedo data of GLASS (Global Land Surface Satellite) products (Liang et al., 2020) to evaluate the WRF simulations. Additionally, we generate snowfall amount data and evaluate the WRF simulated 2 m air temperature based on the TPMFD data set (a high-resolution near-surface Meteorological Forcing Data set for the Third Pole region; Jiang et al., 2023). More details about data are included in Text S1 in Supporting Information S1.

We conduct five simulations from September to next May during 2001–2013 to evaluate the ability of WRF model to simulate snow, air temperature and precipitation on the TP. We also compare different spatial resolutions (10 and 30 km), forcing data (FNL and ERA5 reanalysis data), and land surface schemes (CLM, Noah-MP and SSiB) to investigate the uncertainties in the results (see Table S1 in Supporting Information S1 for more information).

Notably, considering the limited snow on the TP in summer, we define the period from September to next May as the snow season and only analyze the snow characteristics and simulations on the TP during the snow season.

2.2. Snow Phenology and Snowfall Amount

Snow phenology characterizes the seasonal changes of snow cover and features as an indicator of snow cover changes under global warming (Guo et al., 2022; Ke et al., 2016; Lin & Jiang, 2017; Liston & Hiemstra, 2011). Commonly used snow phenology indexes include SCOD (snow cover onset date), SCED (snow cover end date) and SCD (snow cover duration). However, previous researches almost identified snow phenology by fixed threshold (2 cm for SD, 50% for SCF or others), which may be not applicable to the thin snow on the TP (Brown et al., 2007; Gao et al., 2011; Notarnicola, 2020). In this study, we simply develop a set of dynamic snow phenology indexes simply based on the upper and lower quartiles between the maximum and minimum values of snow variables, consistent of OA (onset of accumulation period), OS (onset of stabilization period), P (peak), ES (end of stabilization period), EM (end of melting period). The new indexes can more precisely capture the snow phenology on the TP.

In this study, we also focus on the wet bias on the TP, and it mainly refers to snowfall amount bias during snow season. However, gridded snowfall amount data are missing on the TP. Here we employ dual-threshold temperature method (Chen et al., 2014; Marks et al., 2013) and TPMFD meteorological data to calculate snowfall amount:

$$\text{Snowfall} = \begin{cases} P & , T \le T_S \\ P \times \dfrac{T - T_S}{T_L - T_S} & , T_S < T < T_L \\ 0 & , T \ge T_L \end{cases} \tag{1}$$

P is the total precipitation amount and T is the 2 m air temperature. For this study, we set the liquid and solid precipitation threshold (T_L, T_S) to 2°C and 0°C referring to Kang et al. (1999). We will use the calculated snowfall amount to access the bias in simulated snowfall. However, we are also aware that different rain and snow

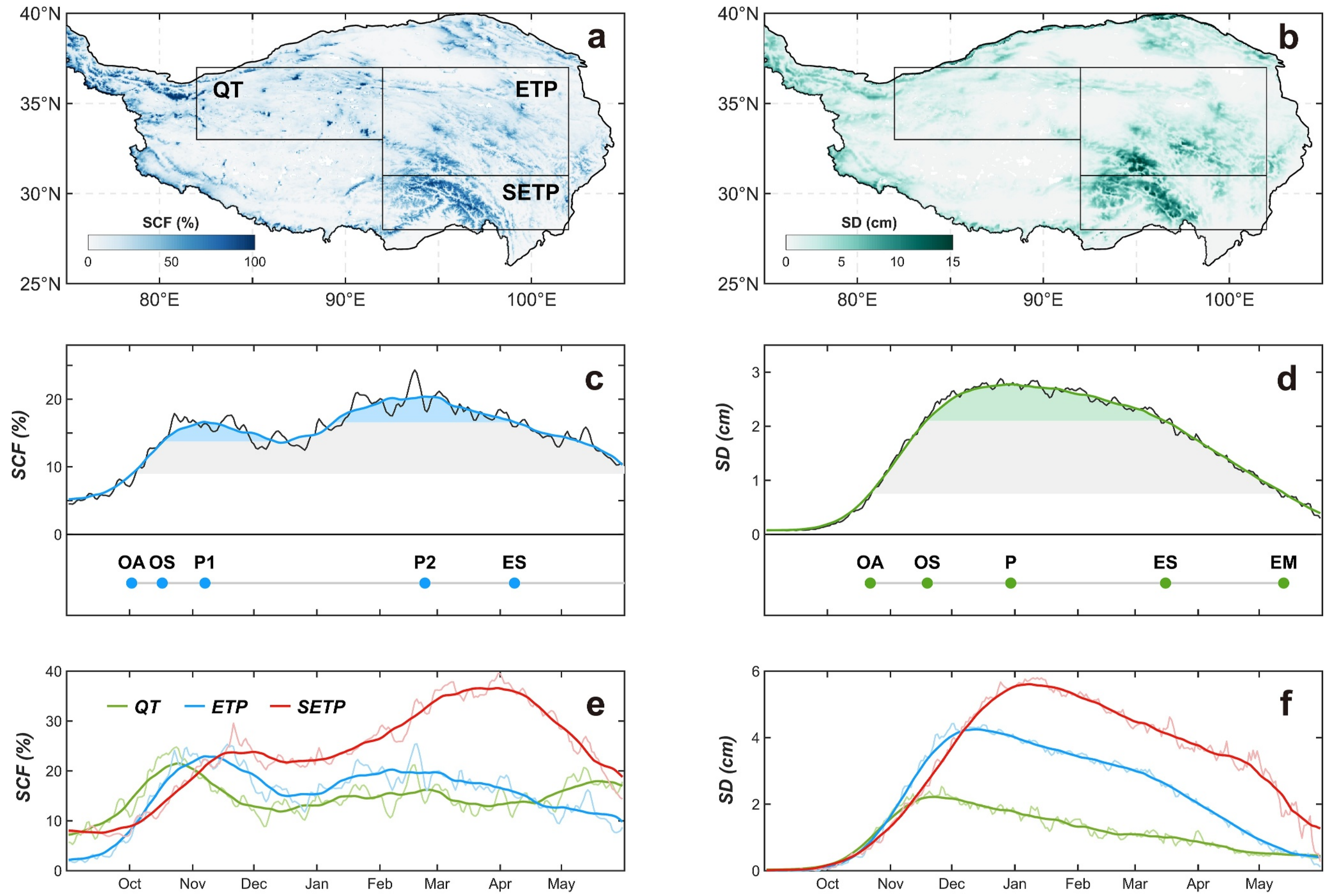

Figure 1. Satellite observed changes of snow cover on the Tibetan Plateau (TP) from September to next May during 2001–2013. (a) Multiyear mean daily change of snow cover fraction (SCF) on the TP during snow season. The three boxes indicate subregions QT, ETP, and SETP, respectively. (c) Annual cycle of regional mean SCF on the TP. The black and blue lines are the original and 30-day moving average time series, separately. And the shades indicate different snow phenology periods. (e) Same as panel (c) but for three subregions. (b, d, f) Same as panels (a, c, e) but for snow depth variation.

identification methods can lead to significant differences in snowfall amounts, which is one of the sources of uncertainty in this study.

3. Results

3.1. Observed Seasonal Changes of TP Snow Cover

Large areas of seasonal snow covers the TP, with an average SD of 1.63 cm and an average SCF of 14.93% in snow season (Figures 1a and 1b). Meanwhile, the TP snow cover is characterized by significant periodic change. Here we employ dynamic snow phenology indexes to indicate this periodic change of TP snow cover (Section 2.2). From Figure 1d, we observe the obvious "accumulation-peak-melting" change of the regional mean SD on the TP during snow season. OA appears in late October while EM appears in mid-May, and the snow cover lasts for about 203 days. Furthermore, TP SD stabilizes from late November to mid-March, peaking at the end of December. However, the annual cycle of SCF presents a unique bimodal characteristic. Specifically, the sub-peak (P1 in Figure 1c) occurs in early November and main peak (P2) occurs in late February. Compared to SD, SCF shows longer duration (more than 248 days) and more intense fluctuations.

TP snow cover has significant spatial heterogeneity due to the complex topography. Satellite observations indicate thin and small snow cover in the central TP, while the snow in the southeastern TP tends to be thicker and larger (Figures 1a and 1b). Here we use the EOF method to explore the spatial and temporal heterogeneity of snow cover variation on the TP.

Figure S1 in Supporting Information S1 shows that there are two main modes for TP snow cover changes, with the peak SCF in mode 1 occurring in late February and peak SD occurring in late December. Mode 1 is the main mode of TP snow cover variation, corresponding to the P2 for SCF and P for SD (Figure 1). Spatially, the positive phase mainly occurs in the eastern and southeastern TP, with no significant phases or even slight negative phases in the central TP. Furthermore, the peak SCF in mode 2 occurs in late October, leading to P1 of SCF variation. The variance contribution rate and peak of SD in mode 2 are too small to lead a bimodal variation.

Notably, phases in mode 2 are opposite in the central-eastern and southeastern TP. Based on it, we divide the TP into three subregions: QT (Qiangtang Plateau/central TP), ETP (eastern TP) and SETP (southeastern TP). We further investigate the seasonal changes of snow cover in three subregions. The SCF peaks first (late October) in the QT, second (early November) in the ETP, and latest (late March) in the SETP (Figure 1e). Meanwhile, the SD also peaks first (late November) in the QT, second (early December) in the ETP, and latest (early January) in the SETP (Figure 1f).

On the whole, the snow cover presents divergent phenological characteristics in different areas of TP and between SCF and SD. However, we do not rule out the possibility that data uncertainty contributes to this phenological discrepancy.

3.2. Evaluation of Snow Simulations in WRF

Regional climate model is one of the important tools for climate researches on the TP, but it remains unclear whether regional climate models can accurately capture the seasonal dynamics of TP snow cover (Gao et al., 2020; Liu & Ma, 2024; Meng et al., 2018). Here we conduct three WRF experiments (WRF-CLM, WRF-NoahMP, WRF-SSiB) during snow season of 2001–2013 to consider the uncertainty of snow parameterization. We only compare the SD due to absence of SCF in the WRF outputs.

Figures 2a–2c show that all three experiments overestimate SD on the whole TP, WRF-CLM by 1.16 cm, WRF-NoahMP by 1.88 cm, and WRF-SSiB by 1.28 cm. The overestimation in SD concentrates in the mountainous areas of northern, western and southeastern TP. However, the three experiments differ in their performance in simulating the spatial distribution of SD, and SD simulated by WRF-CLM experiment has the best spatial correlation with observations (0.50), compared to 0.40 of WRF-NoahMP and 0.44 of WRF-SSiB.

We observe that WRF simulations overall overestimate the peak of TP SD by 137% and delay the peak by about 2 months (Figure 2d). Specifically, WRF simulations underestimate the SD in autumn and overestimate it in following months, leading to the delay and overestimation of peak. Among three experiments, WRF-SSiB performs best on peak simulations but simulates a slower snowmelt process, WRF-CLM near it, and WRF-NoahMP overestimates peak SD the most.

Spatially, the WRF simulations perform differently in three subregions of the TP. In the QT and SETP, the WRF simulation outputs an overestimated and delayed peak SD. The peak SD is the most overestimated in the QT with smallest SD. Surprisingly, all WRF simulations underestimate the peak SD in the ETP. We believe that the underestimation of SD from November to next January resulted in the absence of peak SD. Among three experiments, WRF-CLM performs better in the QT, WRF-NoahMP better in the ETP and SETP, and WRF-SSiB better on the whole TP. Eventually, we choose WRF-CLM for following study based on the mean bias and spatial correlation coefficient of simulated SD (Figures 2a–2c).

As a summary, WRF simulations significantly overestimate SD and delay peak SD on the TP, which differs in different regions and experiments. In WRF simulations, snowfall bias is one of the main possible sources of snow bias.

3.3. Conversion of Snowfall Bias to Snow Amount Bias

Wet bias (positive snowfall bias) exists during snow season on the TP, which directly leads to an overestimated surface snow amount. Here we investigate the relationship between snowfall and snow water equivalent (SWE) on the whole TP (Figure 3) in WRF-CLM experiment. We observe that SWE is slightly underestimated from September to January, and the bias increases rapidly in the following 2 months. The shift in SWE bias matches snow phenology bias in Figure 2d. Notably, the variation of SD bias differs from that of SWE bias, which may be related to snow density.

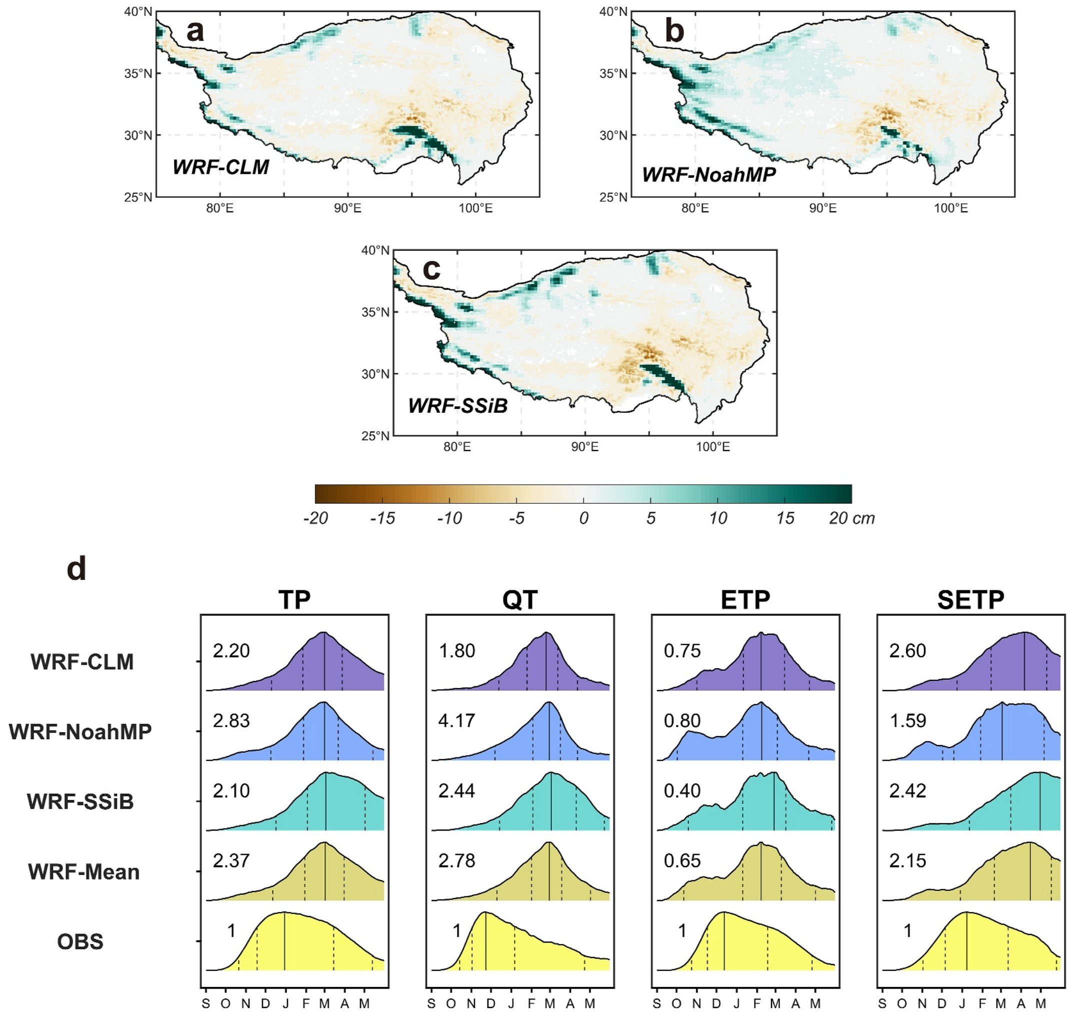

Figure 2. Biases in WRF-simulated snow depth (SD) on the Tibetan Plateau (TP). (a) Multiyear (2001–2013) mean simulated SD bias during snow season in the WRF-CLM experiment. (b) Same as panel (a) but for the WRF-NoahMP experiment. (c) Same as panel (a) but for the WRF-SSiB experiment. (d) Annual cycles of panel observed and simulated SD on the TP and subregions. The WRF-mean indicates the mean value of three experiments. All curves are done as 30-day moving averages and normalized, with numbers indicating the ratio of the peak to observed peak before normalization. Vertical solid and dashed lines indicate the time of occurrence of the five phenological indexes.

Figure 3c shows that positive snowfall bias exists in majority of snow season on the whole TP, the largest bias being in spring exceeding 0.5 mm/d. Before January (Stage 1 in Figure 3d), TP SWE is slightly underestimated despite snowfall being overestimated, which may be related to snowmelt simulations. In contrast, positive snowfall bias efficiently transforms to positive SWE bias from January through mid-March (Stage 2). After mid-March (Stage 3), TP snow enters rapid melting period, resulting in a decreased SWE bias.

We further examine the spatial correlation between snowfall and SWE biases in three stages. In Stage 1, major accumulated snowfall (ACSF) bias occurs in the eastern TP, with maximums above 50 mm/d. Meanwhile, ACSF is slightly underestimated in the QT region. Only positive ACSF bias in small areas of southeastern and edge of TP transforms to positive SWE bias. In Stage 2, ACSF and SWE bias are highly correlated, with spatial correlation coefficients of 0.572. Positive ACSF bias transforms into SWE bias in southeastern and edge of TP, while the transformation is not efficient in central and eastern TP due to rapid changes in thin snow. In Stage 3, ACSF bias is larger, especially in the eastern TP, but as above, snow amount bias has already been decreasing due to ablation.

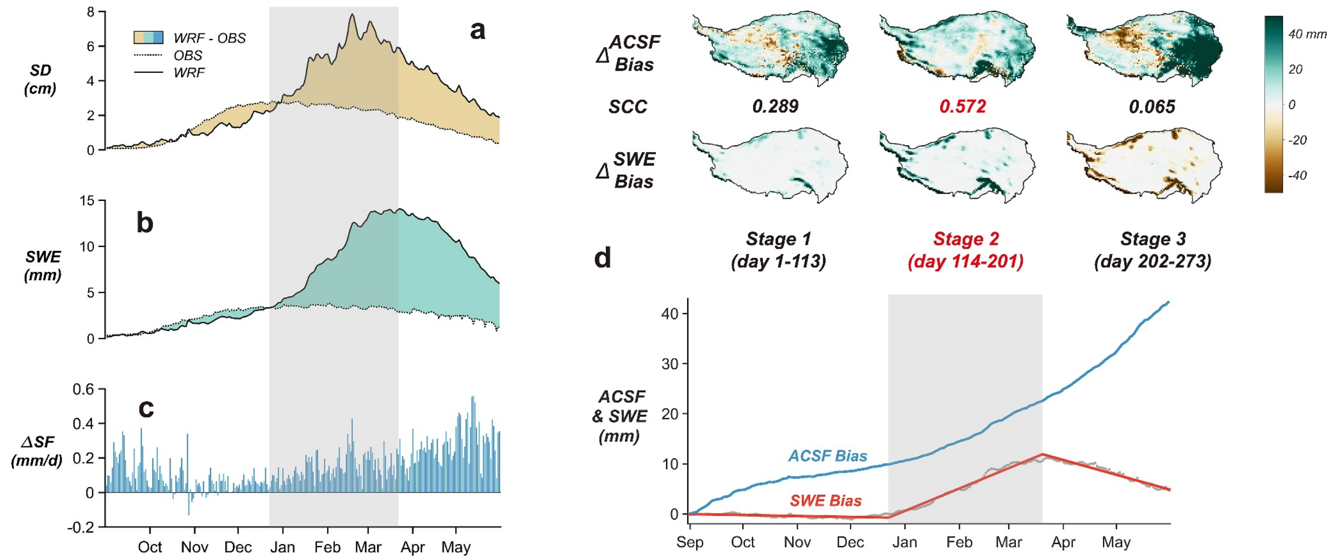

Figure 3. Relationship between biases in WRF-simulated snowfall and snow water equivalent on the whole Tibetan Plateau (TP). (a) Multiyear (2001–2013) regional mean observed and simulated snow depth (SD) during snow season in the WRF-CLM experiment. The color filling indicates the SD bias. (b) Same as panel (a) but for snow water equivalent (SWE). (c) Daily snowfall amount bias (ΔSF) on the whole TP. (d) Changes in the relationship between accumulated snowfall (ACSF) bias and SWE bias. Lower subgraph shows the annual cycle of ACSF and SWE bias, with SWE bias curve obtained by segmental linear fitting based on daily value (gray scatter). The snow season is divided into three stages, and the gray shades indicate the Stage 2. Upper six subgraphs are the spatial changes of ACSF and SWE biases at different stages and their spatial correlation coefficients (SCC).

To avoid the influence of forcing data and resolution on WRF simulation results, here we conduct two additional experiments of higher resolution (10 km) and ERA5 data. We choose the 2003–2004 snow season as the simulation period, which has the largest SD percentage bias (144%), and compared two additional experiments (named ERA5 and FNL10km) with WRF-CLM experiment (named FNL here). Figure S2 shows that ERA5 experiment simulates a larger SWE (0.88 mm) and snowfall (13.34 mm) on the TP compared to FNL experiment. Moreover, higher resolution simulation (FNL10km) brings smaller snowfall bias but larger SWE bias. Nevertheless, we can still draw similar conclusion that TP snowfall bias efficiently transforms into SWE bias in the middle of snow season from Figures S2b and S2c in Supporting Information S1.

Hence, we conclude that the overall wet bias (positive snowfall bias) on the TP is not continually transformed into snow amount bias during snow season, but rather is concentrated and efficiently transformed in mid snow season. We also find the spatial differences for the bias transformation, and we will further discuss the bias transformation processes in three subregions.

4. Discussions and Conclusion

During snow season, positive ACSF bias (wet bias) of 42.41 mm exists across the TP, concentrating in eastern, southeastern and edge of TP (Figure 4). Wet bias occurs mainly in autumn and spring in the ETP (total 69.82 mm), and in the entire snow season in the SETP (total 101.40 mm). However, there is a slight dry bias in the QT (total −7.52 mm), showing a “negative-positive-negative” temporal change in snowfall bias.

As mentioned in Section 3.3, snowfall bias transforms restrictively to SWE bias. In the QT, the bias transformation of snowfall to SWE bias is highly efficient (correlation coefficient of 0.753/0.764), causing underestimation before January and overestimation after January of SWE (Figure S3d in Supporting Information S1). This symmetry bias leads to a larger peak SD in early March and a smaller mean SWE (bias of −0.19 mm). In the ETP, excessive snowfall bias in autumn and spring does not cause significant SWE bias, and even an underestimation of SD occurs in November to January, possibly due to overestimated ablation/sublimation (Figure 4c and Figure S3e in Supporting Information S1). The transformation characteristic in the SETP is similar to that of the entire TP due to the large snow amount. Snowfall bias is almost completely transformed into SWE bias during periods when simulated temperature below 0°C (correlation coefficient of 0.964). To sum up, the transformation

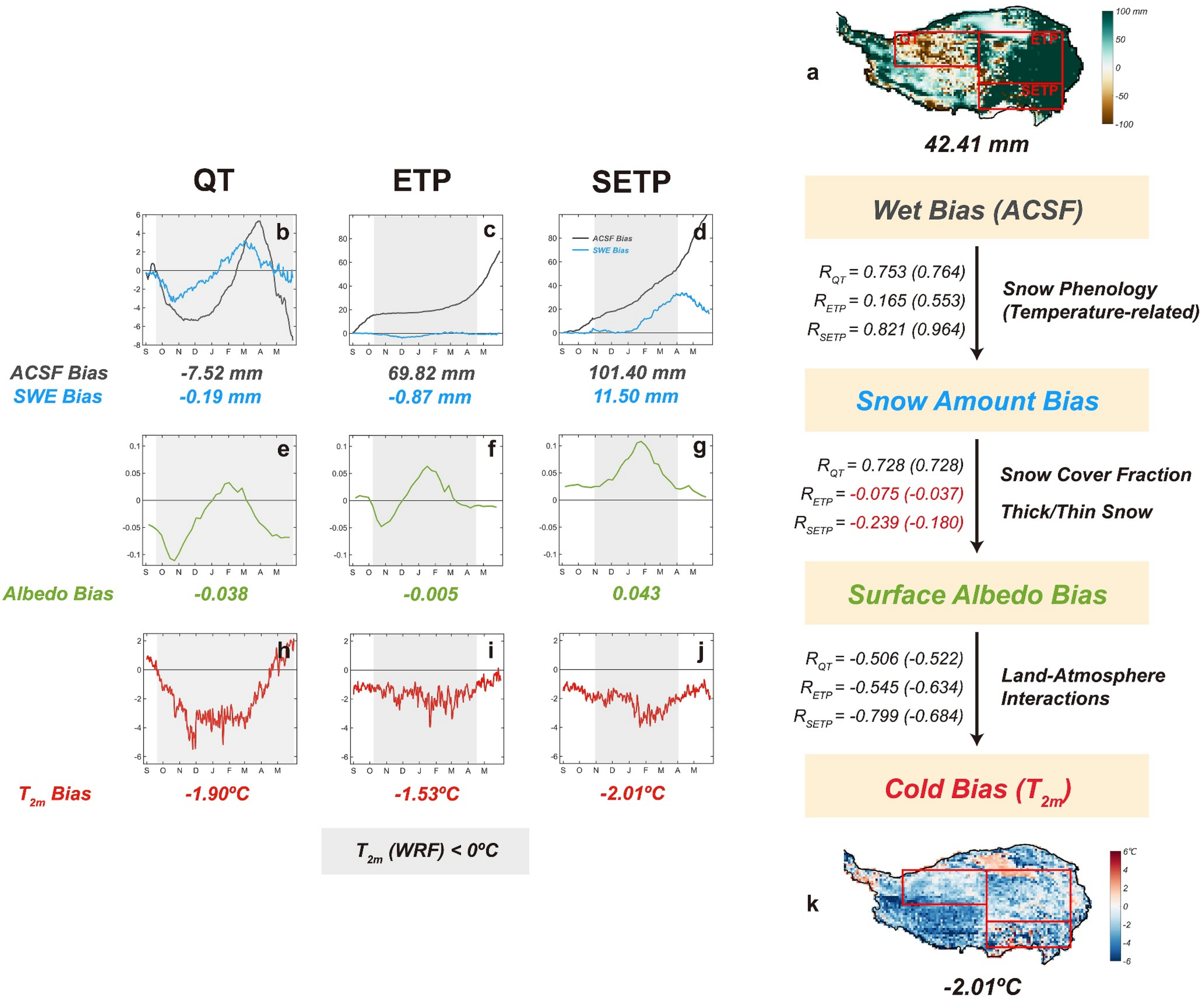

Figure 4. Transformation of wet to cold bias on the Tibetan Plateau (TP) during snow season. (a) Multiyear (2001–2013) mean accumulated snowfall (ACSF) bias on the TP during snow season. Red boxes indicate the location of three subregions. (b–d) Regional mean ACSF and snow water equivalent (SWE) bias in three subregions. (e–g) Regional mean surface albedo bias in three subregions. (h–j) Regional mean 2 m air temperature (T_{2m}) bias in three subregions. (k) Same as panel (a) but for T_{2m} bias. The gray shades indicate the time period when WRF-simulated T_{2m} is less than 0°C. The flow chart shows the step-by-step transformation of wet to cold bias. R indicates the correlation coefficient between the two curves in each transformation, with the correlation coefficient for the time period when WRF-simulated T_{2m} is less than 0°C in brackets. Red R indicates that the correlation fails the test of significance by 0.05, and black R indicates the pass.

of wet bias (positive snowfall bias) to snow amount bias (SWE bias) limited by snow phenology, which is related to temperature. The transformation is more efficient during snow accumulation period.

Snow cover significantly affects TP surface albedo during snow season. In the QT with large areas of thin snow, the transformation of SWE to surface albedo bias is instantly and efficiently (correlation coefficient of 0.728). Notably, the negative surface albedo bias of −0.038 may result from the soil-related systematic bias (of about −0.05). In the ETP and SETP, although the SWE bias induces albedo bias, their temporal correlation is low or even negative.

We observe a significant difference between the simulated and observed "snow amount-albedo" relationship. In observations, change in albedo does not correlate well with SWE, but instead is more consistent with change in SCF (Figure 1e). Our previous study has proved that SCF maintains TP surface albedo change in snow season on the TP, and SD related snow albedo contributes secondarily (Miao et al., 2024). SCF contributes more to albedo change in thick snow areas due to snow albedo with small change, corresponding to the differences between

Figures S3g–S3i in Supporting Information S1. Furthermore, we demonstrated the "de-coupling" of SD and SCF on the TP in previous work. However, current climate models mostly calculate both SCF and snow albedo by snow amount (SWE or SD), leading to the similar tendency among snow amount, SCF and surface albedo on the TP (Figures S3d, S3e, S3g, and S3h in Supporting Information S1). In the SETP with thick snow, the earlier peak of surface albedo than that of SWE may result from the simulated SCF. Eventually, the "snow amount-albedo" relationship restricts the transformation of snow amount to surface albedo bias, but the empirical SCF schemes introduce new biases.

Furthermore, the surface albedo significantly influences the surface air temperature by affecting radiation budget and energy balance processes. From Figures 4e–4j, the albedo bias effectively transforms into instantly and effectively transformed into surface air temperature bias (cold bias) over the TP, with correlation coefficients of −0.506/−0.522, −0.545/−0.634 and −0.799/−0.684 for three subregions. Surprisingly, largest cold bias occurs in the mountainous areas of southwestern TP rather than in the snow-covered areas, which might be related to rocky underlying surface (Yue et al., 2021) and sub-grid terrain radiative effects (Huang et al., 2022). Notably, this bias transformation is grounded in the actual physical processes of snow cover, making it model-independent and generally applicable to different snow conditions. As an example, in the QT region, this bias transformation remains consistent for both extreme snow-rich (2002–2003) and snow-poor (2012–2013) years (Figure S4 in Supporting Information S1). Furthermore, the step-by-step transformation of wet to cold bias is not a unidirectional transfer but consists of feedbacks. For instance, temperature controls the conversion of snowfall to snow amount bias, which in turn changes temperature by affecting albedo.

In conclusion, this study analyzes the snow phenology using satellite observations and evaluates the WRF simulations. We reveals that wet bias on the TP during snow season transforms into positive snow amount bias under the limitation of temperature-related snow phenology. Then, snow amount bias cannot instantly and effectively transform into albedo bias due to the relationship between snow amount, SCF and surface albedo. Eventually, the surface albedo bias induces the cold bias in surface air temperature simulation over the TP. More importantly, the step-by-step transformation of wet to cold bias varies significantly in different regions of the TP.

Our research highlights the spatio-temporally divergent transformation of wet to cold bias on the TP during snow season, providing a novel perspective to understand the intrinsic connection between wet and cold biases. From the point of view of simulation improvements, we believe that reducing the wet bias may not fully address the cold bias, and improving SCF simulations is also crucial.

Data Availability Statement

The daily cloudless MODIS snow area ratio data set of the TP is downloaded at https://data.tpdc.ac.cn/en/data/94a8858b-3ace-488d-9233-75c021a964f0/. The 0.05° snow depth data set for TP is available at https://data.tpdc.ac.cn/en/data/0515ce19-5a69-4f86-822b-330aa11e2a28/. The 0.01° SWE data set for TP is available at https://data.tpdc.ac.cn/en/data/ef039968-7310-4172-8888-8be29d4cfbf0. The GLASS albedo products are available at http://www.glass.umd.edu/Albedo/MODIS/0.05D/. And the TPMFD data set can be found at https://data.tpdc.ac.cn/en/data/44a449ce-e660-44c3-bbf2-31ef7d716ec7.

Acknowledgments
This study is jointly supported by the Second Tibetan Plateau Scientific Expedition and Research Program (STEP) (2019QZKK0103), the National Natural Science Foundation of China (42305033), and the "GeoX" Interdisciplinary Research Funds for the Frontiers Science Center for Critical Earth Material Cycling, Nanjing University (14380114).

References

Brown, R., Derksen, C., & Wang, L. (2007). Assessment of spring snow cover duration variability over northern Canada from satellite datasets. *Remote Sensing of Environment*, *111*(2–3), 367–381. https://doi.org/10.1016/j.rse.2006.09.035

Chen, R., Liu, J., & Song, Y. (2014). Precipitation type estimation and validation in China. *Journal of Mountain Science*, *11*(4), 917–925. https://doi.org/10.1007/s11629-012-2625-x

Chen, X., Liu, Y., & Wu, G. (2017). Understanding the surface temperature cold bias in CMIP5 AGCMs over the Tibetan Plateau. *Advances in Atmosphere Sciences*, *34*(12), 1447–1460. https://doi.org/10.1007/s00376-017-6326-9

Cui, T., Li, C., & Tian, F. (2021). Evaluation of temperature and precipitation simulations in CMIP6 models over the Tibetan Plateau. *Earth and Space Science*, *8*(7), e2020EA001620. https://doi.org/10.1029/2020EA001620

Duan, A., Hu, J., & Xiao, Z. (2013). The Tibetan Plateau summer monsoon in the CMIP5 simulations. *Journal of Climate*, *26*(19), 7747–7766. https://doi.org/10.1175/JCLI-D-12-00685.1

Duan, A., & Wu, G. (2005). Role of the Tibetan Plateau thermal forcing in the summer climate patterns over subtropical Asia. *Climate Dynamics*, *24*(7–8), 793–807. https://doi.org/10.1007/s00382-004-0488-8

Gao, Y., Chen, F., & Jiang, Y. (2020). Evaluation of a convection-permitting modeling of precipitation over the Tibetan Plateau and its influences on the simulation of snow-cover fraction. *Journal of Hydrometeorology*, *21*(7), 1531–1548. https://doi.org/10.1175/JHM-D-19-0277.1

Gao, Y., Xiao, L., Chen, D., Xu, J., & Zhang, H. (2018). Comparison between past and future extreme precipitations simulated by global and regional climate models over the Tibetan Plateau. *International Journal of Climatology*, *38*(3), 1285–1297. https://doi.org/10.1002/joc.5243

Gao, Y., Xie, H., & Yao, T. (2011). Developing snow cover parameters maps from MODIS, AMSR-E, and blended snow products. *Photogrammetric Engineering & Remote Sensing*, *77*(4), 351–361. https://doi.org/10.14358/PERS.77.4.351

Gao, Y., Xu, J., & Chen, D. (2015). Evaluation of WRF mesoscale climate simulations over the Tibetan Plateau during 1979–2011. *Journal of Climate*, *28*(7), 2823–2841. https://doi.org/10.1175/jcli-d-14-00300.1

Gu, C., Huang, A., Zhang, Y., Yang, B., Cai, S., Xu, X., et al. (2022). The wet bias of RegCM4 over Tibet Plateau in summer reduced by adopting the 3D sub-grid terrain solar radiative effect parameterization scheme. *Journal of Geophysical Research: Atmospheres*, *127*(21), e2022JD037434. https://doi.org/10.1029/2022JD037434

Guo, H., Wang, X., Guo, Z., & Chen, S. (2022). Assessing snow phenology and its environmental driving factors in Northeast China. *Remote Sensing*, *14*(2), 262. https://doi.org/10.3390/rs14020262

Hu, W., Duan, A., Li, Y., & He, B. (2016). The intraseasonal oscillation of eastern Tibetan Plateau precipitation in response to the summer Eurasian wave train. *Journal of Climate*, *29*(20), 7215–7230. https://doi.org/10.1175/JCLI-D-15-0620.1

Huang, A., Gu, C., Zhang, Y., Li, W., Zhang, L., Wu, Y., et al. (2022). Development of a clear-sky 3D sub-grid terrain solar radiative effect parameterization scheme based on the mountain radiation theory. *Journal of Geophysical Research: Atmospheres*, *127*(13), e2022JD036449. https://doi.org/10.1029/2022JD036449

Jiang, Y., Yang, K., Qi, Y., Zhou, X., He, J., Lu, H., et al. (2023). TPHiPr: A long-term (1979–2020) high-accuracy precipitation dataset (1/30∘, daily) for the third Pole region based on high-resolution atmospheric modeling and dense observations. *Earth System Science Data*, *15*(2), 621–638. https://doi.org/10.5194/essd-15-621-2023

Kang, E., Cheng, G., Lan, Y., & Jin, H. (1999). A model for simulating the response of runoff from the mountainous watersheds of inland river basins in the arid area of northwest China to climatic changes. *Science in China Series D: Earth Sciences*, *42*(S1), 52–63. https://doi.org/10.1007/BF02878853

Ke, C., Li, X., Xie, H., Ma, D., Liu, X., & Kou, C. (2016). Variability in snow cover phenology in China from 1952 to 2010. *Hydrology and Earth System Sciences*, *20*(2), 755–770. https://doi.org/10.5194/hess-20-755-2016

Kukulies, J., Chen, D., & Curio, J. (2021). The role of mesoscale convective systems in precipitation in the Tibetan Plateau region. *Journal of Geophysical Research: Atmospheres*, *126*(23), e2021JD035279. https://doi.org/10.1029/2021JD035279

Lalande, M., Ménégoz, M., Krinner, G., Naegeli, K., & Wunderle, S. (2021). Climate change in the High Mountain Asia in CMIP6. *Earth System Dynamics*, *12*(4), 1061–1098. https://doi.org/10.5194/esd-12-1061-2021

Lee, W., Li, J., Xu, K., Suhas, E., Jiang, J., Wang, Y., et al. (2019). Relating precipitating ice radiative effects to surface energy balance and temperature biases over the Tibetan Plateau in winter. *Journal of Geophysical Research: Atmospheres*, *124*(23), 12455–12467. https://doi.org/10.1029/2018JD030204

Li, P., Furtado, K., Zhou, T., Chen, H., Li, J., Guo, Z., & Xiao, C. (2020). The diurnal cycle of East Asian summer monsoon precipitation simulated by the Met Office Unified Model at convection-permitting scales. *Climate Dynamics*, *55*(1–2), 131–151. https://doi.org/10.1007/s00382-018-4368-z

Liang, S., Cheng, J., Jia, K., Jiang, B., Zhou, J., Xiao, Z., et al. (2020). The Global Land Surface Satellite (GLASS) product suite. *Bulletin of the American Meteorological Society*, *102*(2), 1–37. https://doi.org/10.1175/BAMS-D-18-0341.1

Lin, Y., & Jiang, M. (2017). Maximum temperature drove snow cover expansion from the Arctic, 2000-2008. *Scientific Reports*, *7*(1), 15090. https://doi.org/10.1038/s41598-017-15397-3

Liston, G. E., & Hiemstra, C. A. (2011). The changing cryosphere: Pan-Arctic snow Trends (1979-2009). *Journal of Climate*, *24*(21), 5691–5712. https://doi.org/10.1175/JCLI-D-11-00081.1

Liu, L., & Ma, Y. (2024). Improvement of albedo and snow-cover simulation during snow events over the Tibetan Plateau. *Monthly Weather Review*, *152*(3), 705–724. https://doi.org/10.1175/MWR-D-23-0083.1

Marks, D., Winstral, A., Reba, M., Pomeroy, J., & Kumar, M. (2013). An evaluation of methods for determining during-storm precipitation phase and the rain/snow transition elevation at the surface in a mountain basin. *Advances in Water Resources*, *55*, 98–110. https://doi.org/10.1016/j.advwatres.2012.11.012

Meng, X., Lyu, S., Zhang, T., Zhao, L., Li, Z., Han, B., et al. (2018). Simulated cold bias being improved by using MODIS time-varying albedo in the Tibetan Plateau in WRF model. *Environmental Research Letters*, *13*(4), 044028. https://doi.org/10.1088/1748-9326/aab44a

Miao, X., Guo, W., Li, W., Cao, Y., Ge, J., & Qiu, B. (2024). Instant response of Tibetan Plateau surface albedo to snow coverage and depth in snow season. *Geophysical Research Letters*, *51*(3), e2023GL108010. https://doi.org/10.1029/2023GL108010

Miao, X., Guo, W., Qiu, B., Lu, S., Zhang, Y., Xue, Y., & Sun, S. (2022). Accounting for topographic effects on snow cover fraction and surface albedo simulations over the Tibetan Plateau in winter. *Journal of Advances in Modeling Earth Systems*, *14*(8), e2022MS003035. https://doi.org/10.1029/2022MS003035

Notarnicola, C. (2020). Hotspots of snow cover changes in global mountain regions over 2000-2018. *Remote Sensing of Environment*, *243*, 111781. https://doi.org/10.1016/j.rse.2020.111781

Orsolini, Y., Wegmann, M., Dutra, E., Liu, B., Balsamo, G., Yang, K., et al. (2019). Evaluation of snow depth and snow cover over the Tibetan Plateau in global reanalyses using in situ and satellite remote sensing observations. *The Cryosphere*, *13*(8), 2221–2239. https://doi.org/10.5194/tc-13-2221-2019

Salunke, P., Jain, S., & Mishra, S. K. (2019). Performance of the CMIP5 models in the simulation of the Himalaya-Tibetan Plateau monsoon. *Theoretical and Applied Climatology*, *137*(1–2), 909–928. https://doi.org/10.1007/s00704-018-2644-9

Su, F., Duan, X., Chen, D., Hao, Z., & Cuo, L. (2013). Evaluation of the global climate models in the CMIP5 over the Tibetan Plateau. *Journal of Climate*, *26*(10), 3187–3208. https://doi.org/10.1175/JCLI-D-12-00321.1

Tang, Z., Wang, J., Li, H., & Yan, L. (2013). Spatiotemporal changes of snow cover over the Tibetan Plateau based on cloud-removed moderate resolution imaging spectroradiometer fractional snow cover product from 2001 to 2011. *Journal of Applied Remote Sensing*, *7*(1), 073582. https://doi.org/10.1117/1.JRS.7.073582

Usha, K. H., Nair, V. S., & Babu, S. S. (2020). Modeling of aerosol induced snow albedo feedbacks over the Himalayas and its implications on regional climate. *Climate Dynamics*, *54*(9–10), 4191–4210. https://doi.org/10.1007/s00382-020-05222-5

Wan, B., Gao, Z., Chen, F., & Lu, C. (2017). Impact of Tibetan-plateau surface heating over on persistent extreme precipitation events in southeastern China. *Monthly Weather Review*, *145*(9), 3485–3505. https://doi.org/10.1175/MWR-D-17-0061.1

Wang, Z., Duan, A., & Wu, G. (2014). Time-lagged impact of spring sensible heat over the Tibetan Plateau on the summer rainfall anomaly in East China: Case studies using the WRF model. *Climate Dynamics*, *42*(11–12), 2885–2898. https://doi.org/10.1007/s00382-013-1800-2

Wu, G., Liu, Y., Zhang, Q., Duan, A., Wang, T., Wan, R., et al. (2007). The influence of mechanical and thermal forcing by the Tibetan Plateau on Asian climate. *Journal of Hydrometeorology*, *8*(4), 770–789. https://doi.org/10.1175/JHM609.1

Wu, G., & Zhang, Y. (1998). Tibetan Plateau forcing and the timing of the monsoon onset over South Asia and the South China Sea. *Monthly Weather Review*, *126*(4), 913–927. https://doi.org/10.1175/1520-0493(1998)126<0913:TPFATT>2.0.CO;2

Yan, D., Ma, N., & Zhang, Y. (2021). Development of a fine-resolution snow depth product based on the snow cover probability in the Tibetan Plateau: Validations and spatial-temporal analyses. *Journal of Hydrology*, *604*, 127027. https://doi.org/10.1016/j.jhydrol.2021.127027

Yan, D., & Zhang, Y. (2022). A daily, 0.01° Snow water equivalent dataset for Tibetan Plateau (2000-2018). *National Tibetan Plateau / Third Pole Environment Data Center*. https://doi.org/10.11888/Cryos.tpdc.272289

Yang, B., Zhou, Y., Zhang, Y., Huang, A., Qian, Y., & Zhang, L. (2018). Simulated precipitation diurnal cycles over East Asia using different CAPE-based convective closure schemes in WRF model. *Climate Dynamics*, *50*(5–6), 1639–1658. https://doi.org/10.1007/s00382-017-3712-z

Yeh, T. C. (1950). The circulation of the high troposphere over China in the winter of 1945-46. *Tellus*, *2*(3), 173–183. https://doi.org/10.3402/tellusa.v2i3.8548

Yu, E., Sun, J., Chen, H., & Xiang, W. (2015). Evaluation of a high-resolution historical simulation over China: Climatology and extremes. *Climate Dynamics*, *45*(7–8), 2013–2031. https://doi.org/10.1007/s00382-014-2452-6

Yue, S., Yang, K., Lu, H., Zhou, X., Chen, D., & Guo, W. (2021). Representation of stony surface-atmosphere interactions in WRF reduces cold and wet biases for the Southern Tibetan Plateau. *Journal of Geophysical Research: Atmospheres*, *126*(21), e2021JD035291. https://doi.org/10.1029/2021JD035291

Zhou, X., Yang, K., Beljaars, A., Li, H., Wang, Y., & Huang, B. (2019). Dynamical impact of parameterized turbulent orographic form drag on the simulation of winter precipitation over the western Tibetan Plateau. *Climate Dynamics*, *53*(16), 707–720. https://doi.org/10.1007/s00382-019-04628-0

Zhou, X., Yang, K., Ouyang, L., Wang, Y., Prein, A., Li, X., et al. (2021). Added value of kilometer-scale modeling over the third pole region: A cordex-cptp pilot study. *Climate Dynamics*, *57*(7–8), 1673–1687. https://doi.org/10.1007/s00382-021-05653-8

Zhu, Y., & Yang, S. (2020). Evaluation of CMIP6 for historical temperature and precipitation over the Tibetan Plateau and its comparison with CMIP5. *Advances in Climate Change Research*, *11*(3), 239–251. https://doi.org/10.1016/j.accre.2020.08.001